Part A: English Edition

Journal of Textiles and Polymers

Vol. 11, No. 1, 43-55, January 2023

https://doi.org/10.48302/jtp.2023.407257.1267

ORIGINAL PAPER

Geometry Modeling and Simulation of Low-Velocity Impact Behavior of Foam-Based Composite Reinforced with Warp-Knitted Spacer Fabric

Amir Hossein Dodankeh and Hadi Dabiryan*

Received: 16 July 2023, Accepted: 9 September 2023

***Abstract*- In the present study, low-velocity impact behavior of foam-based composites reinforced with warp-knitted spacer fabrics (WKSF) was numerically simulated. Spacer fabrics are recently used in new applications such as transportation and construction industries due to their unique properties. For this purpose, at first, easy-to-use mathematical equations were developed to model the geometry of WKSFs as reinforcement. The low-velocity impact behavior of composites reinforced with WKSF with different height, cell-sized and facing or non-facing position of hexagonal cells was analyzed numerically. Stress analysis of samples after impact showed that composites reinforced with high thickness, small cell size, and non-facing position of hexagonal cells have better impact performance than those with low thickness, big cell size, and facing hexagonal cells. Also, the maximum error of 9.8% confirms that the generated model and numerical simulation can well predict the low-velocity impact behavior of WKSF-reinforced foam-based composites.**

***Keywords*: low velocity impact, foam-based composite, warp-knitted spacer fabric, FE simulation**

I. INTRODUCTION

To analyze the mechanical behavior of composite reinforced with fabrics, we need to generate a precise geometrical model. Considering the complexity of fabric structures, it is necessary to make some simplifying assumptions. These assumptions are related to the type of fabric. In 3D fabrics such as warp/weft-knitted spacer fabrics, the construction consists different parts i.e., top/bottom layers and spacer yarns. To model their geometry, at first, different parts should be considered, separately. Thereafter, the generated parts are assembled to make the whole structure.

There is a history of modeling the different fabrics geometry [1-5]. The ideal geometry of the plain weave by rigorous formula is given by Pierce [1]. Laef and Glaskin [2] presented a geometrical model of a plain knitted loop as a basis for a mathematical description of the dimensional properties of a plain knitted fabric. Kemp [3] extended Peirce's earlier research by working on non-circular sections of yarns. Munden [4] showed that with these assumptions, the dimensional and weight properties of the knitted fabric in a relaxed state are determined uniquely by the length of yarn in the stitch. Hearl and Shanahan [5] described an energy method to calculate the fabric mechanics.

Some previous models have been developed by researchers [6-9]. Vassikiadis [6], proposed a model based on the assumptions of the ideal elastic yarn and the elastic energy minimization of the yarns composing the relaxed fabrics. Dolatabadi and Kovar [7] developed a 3D model of plain weave fabric before deformation. Jeddi *et al.* [8] presented a theoretical analysis of a model of plain-weft-knitted fabric subjected to uniaxial loading in either direction. Dabiryan and Jeddi [9] established a 3D straight line model for two-guide-bar warp knitted fabrics. Recently, several attempts have been performed to model the 3D fabrics using different methods [10-12]. Kyosev [10] studied the 3D geometry of braided fabrics and provided a generalized geometrical approach for modeling braided structures and the 3D forming of textiles in composite manufacturing. Kurbak [11] generated a geometrical model for weft-knitted spacer fabrics. Delavari and Dabiryan [12] developed a mathematical and numerical model for

A.H. Dodankeh and H. Dabiryan
Department of Textile Engineering, Amirkabir University of Technology
Tehran, Iran.

Correspondence should be addresses to H. Dabiryan
e-mail: dabiryan@aut.ac.ir

1×1-rib weft-knitted spacer fabrics.

Analyzing the mechanical properties of composites particularly composites reinforced with 3D fabrics such as WKSF has received the attention of many researchers. The most basic research on the impact behavior of foams began with the presentation of a simple model, known as the Maxwell model, consisting of ball, spring, and dashpot [13]. A dimensionless parameter was introduced in this model to express the impact behavior and energy absorption of foams. The use of dimensionless parameters simplifies the description of foam systems and provides a suitable method for comparing systems with very different properties. It also facilitates the qualitative determination of energy absorption properties. Gibson and Ashby [14] stated that the mechanical properties of foams generally depend on the base liquid, relative density, and foam cell geometry. Allen *et al.* [15] studied the effect of low-energy impact on conventional open-cell foams and auxetic foams. Their results showed the samples with auxetic properties exhibited a significant decrease of six times in peak acceleration, indicating promise for use in impact protection equipment such as shin or thigh guards for sports gear. Dabiryan *et al.* [16] investigated the impact behavior of composites reinforced with weft-knitted spacer fabrics and studied the effect of fabric geometry using an analytical model based on the energy method. Li *et al.* [17] evaluated the impact force reduction of weft-knitted spacer structures with silicone tube and foam inlays for cushioning insoles. The study found that these inlays can effectively enhance the impact force reduction of the 3D spacer fabrics, Hasanalizadeh and Dabiryan [18] developed an analytical model to predict the low-velocity impact properties of sandwich-structured composites reinforced with weft-knitted spacer fabric. The model utilized Hertz contact law. Zhi *et al.* [19] used a warp-knitted spacer fabric as syntactic foam reinforcement and measured the compression modulus of this composite. Their results showed that the use of WKSF as a reinforcement improves the compressive modulus of the reinforced foam by at least 15% compared to neat syntactic foam. Delavari and Dabiryan [20] investigated the effect of Z-fiber orientation on the bending behavior of sandwich composites through numerical and experimental methods. Their results showed that in the transverse direction, Z-fibers played a major role in the bending behavior of these composites, whereas in the longitudinal direction, the layers were found to play the main role. Ghorbani *et al.* [21] used WKSFs as reinforcement of cement-based composites to enhance the bending behavior of concrete beam.

This study tries to develop easy-to-use mathematical equations to model the geometry of Warp-Knitted Spacer Fabrics (WKSFs) as reinforcements of sandwich composites. Then, the generated model is used to simulate the low-velocity impact behavior of foam-based composites by ABAQUS software. The numerical results are compared to the results of drop-hammer impact test to check the accuracy of conducted simulation.

II. MODELING THE GEOMETRY OF WKSF

Warp-knitted spacer fabrics (WKSFs) is a type of 3D fabrics that consists of two separate weft-knitted layers, joined together by spacer yarns. Fig. 1 shows the schematic of WKSF and its different parts. As shown, the top/bottom layers morphology corresponds to the hexagonal cells.

A. Mathematical Equations

As shown in Fig. 1, the WKSF has two main parts which are individually modeled in this research. The top/bottom layers have hexagonal cells and the pile yarns are as curved rods. To accurately model a hexagon, it is necessary to know the angle of the hexagon (θ) as well as the dimensions of l, h, and t as shown in Fig. 2.

B. Top/Bottom Layer Geometry

It is well known that the geometry of knitted structures is expressed by CPC (course per centimeters), WPC (wale per centimeters) or yarn diameter (d). In the spacer fabrics, the thickness of fabrics should also be considered. Since, the hexagonal cells are formed by loops, their geometry is defined using these parameters. The height of each loop in the warp-knitted fabric is equal to c=1/CPC. Therefore, the size of the sides, i.e., l and h can be expressed as

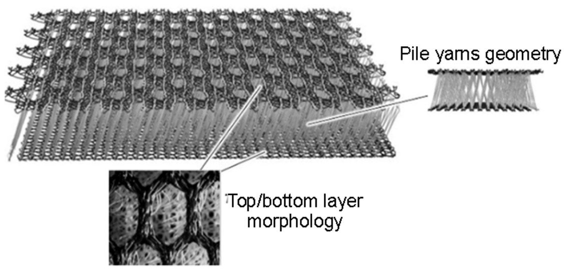

Fig. 1. Schematic representation of WKSFs.

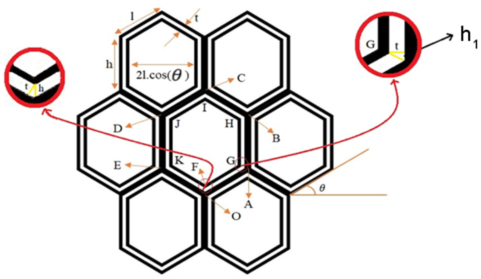

Fig. 2. Hexagonal cell of top/bottom layers.

multiples of c. The origin of the coordinates is denoted by O, and Eq. (1) shows the coordinates of the end points of the line OA. The size of the vertical component of the line OA, n, is equal to the w=1/WPC. Hence, we can write:

$$\begin{cases} x = n_{OA} \times c \times \cot(\theta) \\ y = n_{OA} \times c \end{cases} \tag{1}$$

where the value of n_{OA} represents the number of loops on the side OA. The coordinates of the starting point of the line AB are the same as the end point of line OA. Eq. (2) shows the coordinates of the end point of side AB as below:

$$\begin{cases} x = n_{OA} \times c \times \cot(\theta) \\ y = n_{OA} \times c + n_{AB} \times c \end{cases} \tag{2}$$

Also, the coordinates of the endpoint of line BC are according to Eq. (3):

$$\begin{cases} x = 0 \\ y = n_{OA} \times c + n_{AB} \times c + n_{BC} \times c \end{cases} \tag{3}$$

Based on Fig. 2, the values of the starting and ending points of lines CD, DE, and EO can be calculated by Eqs. (4), (5), and (6), respectively:

$$\begin{cases} x = -n_{OA} \times c \times \cot(\theta) \\ y = n_{OA} \times c + n_{AB} \times c \end{cases} \tag{4}$$

$$\begin{cases} x = -n_{OA} \times c \times \cot(\theta) \\ y = n_{OA} \times c \end{cases} \tag{5}$$

$$\begin{cases} x = 0 \\ y = 0 \end{cases} \tag{6}$$

Using Eqs. (1) to (6), the geometry of the outer line of hexagonal cells that forms the cell walls has been mathematically defined. Considering the width of hexagons' wall, the inner line of hexagonal cells is derived. The width of cell walls, t, is equal to four times of yarn diameter, d_2, according to the Chamberlin's theory [26]. Since we are dealing with double-layered fabrics, twice the diameter of the pile yarn, d_1, is added the width due to the presence of connecting yarns in the background loop. Therefore, the value of t is equal to Eq. (7):

$$t = 4 \times d_2 + 2 \times d_1 \tag{7}$$

To derive the equations for the inner hexagons, it is sufficient to add the thickness or loop width to the above equations.

Based on Fig. 2, the starting point of the inner hexagon has a vertical component equal to the value of h, which is obtained as follow:

$$h = \frac{t}{\cos\theta} \tag{8}$$

Also, the coordinates of the starting point of line FG are:

$$\begin{cases} x = 0 \\ y = h \end{cases} \tag{9}$$

The intersection of lines FG and GH is shown as h_1, which aims to maintain the thickness. The value of h_1 is obtained according to Eq. (10):

$$h_1 = t \times \tan\theta \tag{10}$$

Also, the coordinates of the starting point of line GH are:

$$\begin{cases} x = n_{OA} \times c \times \cot(\theta) - t \\ y = n_{OA} \times c + n_{AB} \times c + h_1 \end{cases} \tag{11}$$

Similarly, considering the constraint of constant thickness, the coordinates of the endpoints of lines HI, IJ, JK, and KF are expressed by Eqs. (12) to (15):

$$\begin{cases} x = 0 \\ y = n_{OA} \times c + n_{AB} \times c + n_{BC} \times c - h_1 \end{cases} \tag{12}$$

$$\begin{cases} x = -n_{OA} \times c \times \cot(\theta) + t \\ y = n_{OA} \times c + n_{AB} \times c - h_1 \end{cases} \tag{13}$$

$$\begin{cases} x = -n_{OA} \times c \times \cot(\theta) + t \\ y = n_{OA} \times c + h_1 \end{cases} \tag{14}$$

$$\begin{cases} x = 0 \\ y = h \end{cases} \tag{15}$$

Based on observations and knitting patterns, the connecting threads emerge from the lower part of the circular warp loop and return to the lower part of the circular warp loop after creating the connecting loop. The side view of the intersection between the pile yarn and the layer's yarn is shown in Fig. 3.

Based on Fig. 3, the thickness of layer is calculated as below:

$$T_L = d_2 + \cos(\alpha) d_1 \tag{16}$$

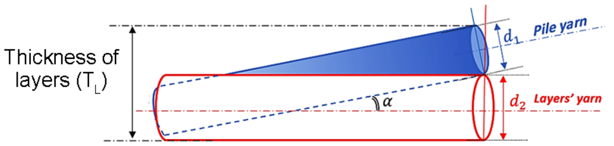

Fig. 3. Schematic side view of the intersection between the pile yarns and the background yarns.

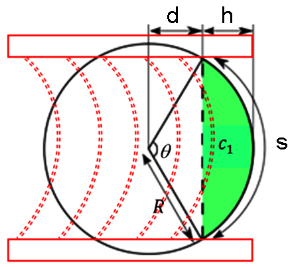

Fig. 4. Geometry of pile yarn as a part of circle.

The angle of the hexagonal cell can be calculated by considering the number of loops (n) per unit length (m), according to Eq. (17):

$$\theta = \cot^{-1}\left(\frac{n}{2\times m\times c}\right) \tag{17}$$

C. Pile Yarn Geometry

Based on the real photos of WKSF structures, the pile yarns have formed an arc as part of a circle. According to sections in Fig. 4.

In all samples, the height of the distance between top and bottom layers is equal to the value of c_1 as shown in Fig. 4. Therefore, the value of the radius of the circle that forms the pile yarns can be calculated as follows:

$$R = \frac{h}{2} + \left(\frac{c_1^2}{8\times h}\right) \tag{18}$$

III. FEM MODELING

Given that the geometry of WKSF has been fully describe mathematically using Eqs. (1) to (18), by converting these equations into programming code in Python and running them in ABAQUS software, the components of the fabric can be modeled. Using derived equations, the geometry of hexagonal cells and pile yarns was simulated in ABAQUS software. In the material section for the background foam, the property of low-density foam extracted from the pressure chart of the used foam was used. Also, the polyester material of the WKSF yarns was considered elastic and from the properties obtained from the tensile test of the yarns. Fig. 5 shows the steps of generating the part of hexagonal cell.

Regarding the geometry proposed for the pile yarns and developed equations, the part of pile yarns was created in software environment. Fig. 6 shows the different views of generated model for the pile yarns.

The geometry of a unit-cell was generated by tie command in software as shown in Fig. 7.

The structure of WKSF was created by assembling the generated unit-cells. Fig. 8 shows the geometrical model for the WKSF structures. The boundary conditions of the target sample were considered as four sides clamp. The impactor was modeled according to the experimental data in the ABAQUS software. The impactor is made of steel in the form of a flat-bottomed cylinder with a diameter of 26 mm and a weight of 2.707 kg. The initial energy of all test samples was considered equal to 5 J, and the impactor fell on the target from a height corresponding to this energy without initial speed.

A. Developing the Model for Different Structures

Considering the geometrical parameters of WKSFs, different structures can be designed and produced. Here, some geometrical parameters at two states were considered as below:

- Height of pile yarns (high/low);
- Size of hexagonal cells (big/small) and
- Position of cells in top and bottom layers (facing/non-facing).

Fig. 9 shows the aforementioned structural parameters demonstrated on the WKSF.

The states of cell positions are shown in Fig. 10. As shown in Fig. 10a, in facing position, the hexagonal cells

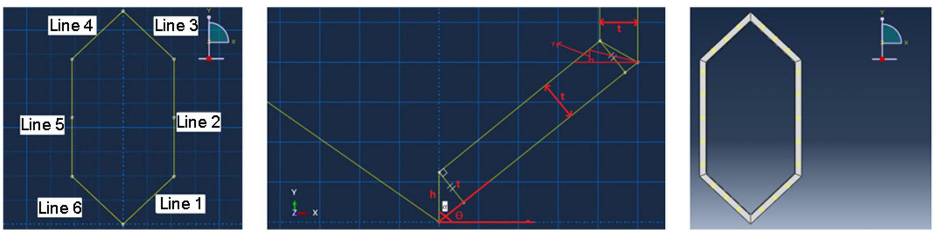

(a) (b) (c)

Fig. 5. Steps of generating hexagonal cell geometry: (a) drawing the sides, (b) thickening the sides, and (c) generating the cell.

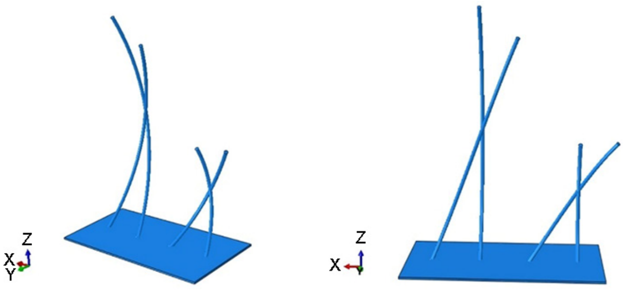

(a) (b)

Fig 6. Different views of part created for pile yarns: (a) transverse direction and (b) longitudinal direction.

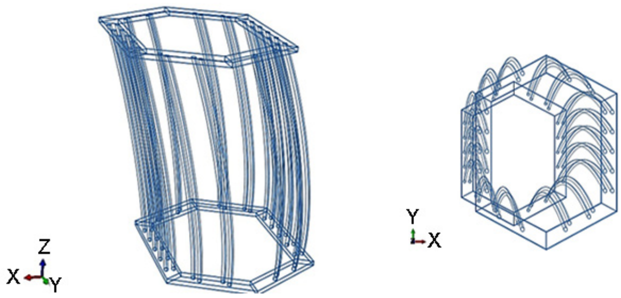

(a) (b)

Fig. 7. The model generated for unit-cell: (a) side view and (b) top view.

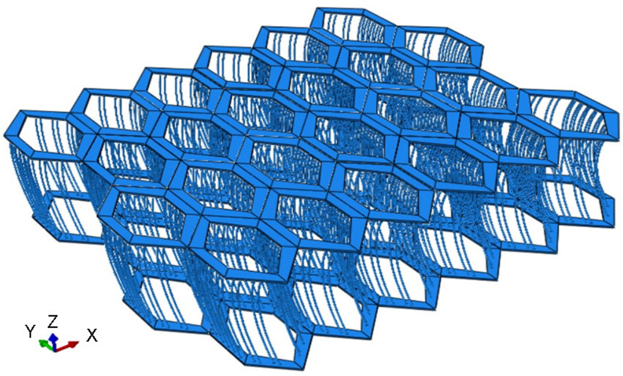

Fig. 8. The model generated for the geometry of WKSFs.

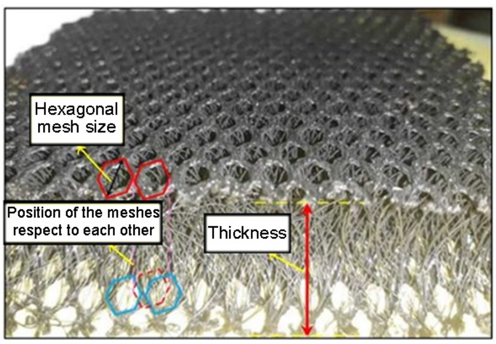

Fig. 9. Structural parameters of WKSF.

in top and bottom layers are exactly face to face, while in non-facing position, they are not positioned face to face (Fig. 10b).

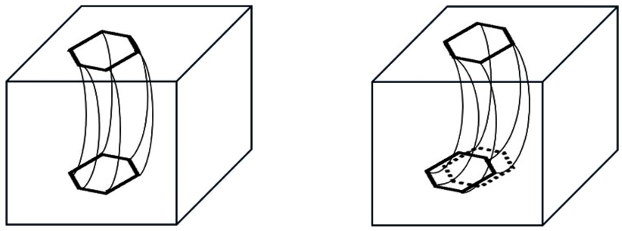

(a) (b)

Fig. 10. Cell positions at top/bottom layer: (a) facing position and (b) non-facing position.

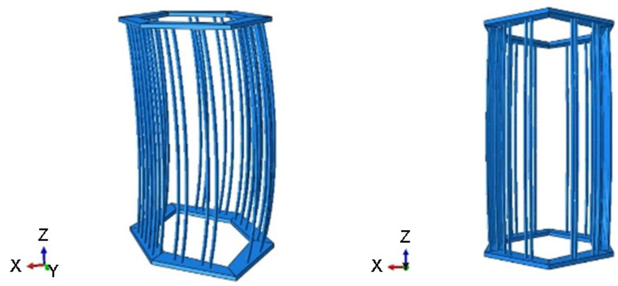

(a) (b)

Fig. 11. Generated model for unit-cell of facing position: (a) transverse direction and (b) longitudinal direction.

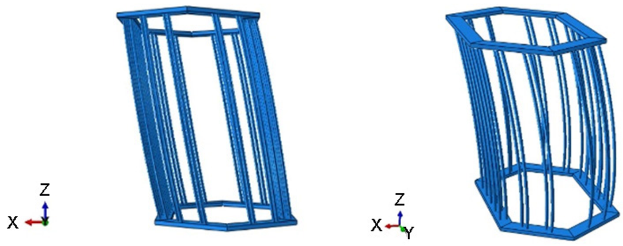

(a) (b)

Fig. 12. Generated model for unit-cell of non-facing position: (a) transverse direction and (b) longitudinal direction.

The model generated for both facing and non-facing positions of a unit-cell are shown in Figs. 11 and 12, respectively.

Considering the structural parameters of WKSFs, different types of reinforcements were designed which their coding system can be found in Table I. According to Table I, the BHN is a coding system example that describes a WKSF sample with big cell-size, high thickness and non-

TABLE I

CODING SYSTEM FOR THE PRODUCED SPACER FABRICS

Item	State	Specified code
Cell size	Big	B
	Small	S
Thickness	High	H
	Low	L
Hole positions	Facing	F
	Non-facing	N

TABLE II
CODING OF MODELED COMPOSITES

Sample's code	Description		
	Size of cell	Height of pile yarns	Position of hexagonal cell
BLN	Big	Low	Non-facing
BHN	Big	High	Non-facing
SHN	Small	High	Non-facing
BLF	Big	Low	Facing
BHF	Big	High	Facing

facing cell position. The nominal thickness value is 14 mm in high thickness samples and 7 mm in low thickness samples.

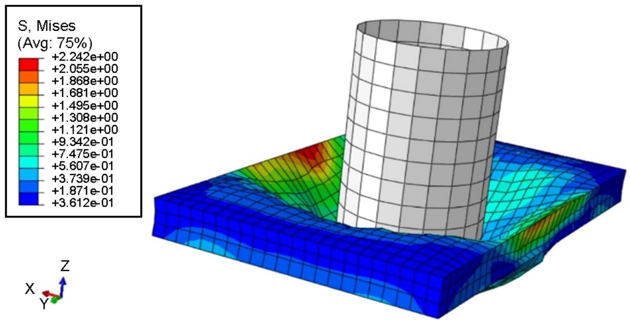

Fig. 13. Von Mises stress in BLF sample.

B. Numerical Simulation of Low-Velocity Impact Behavior

The numerical simulation of the low-velocity impact behavior of foam-based composites was performed using

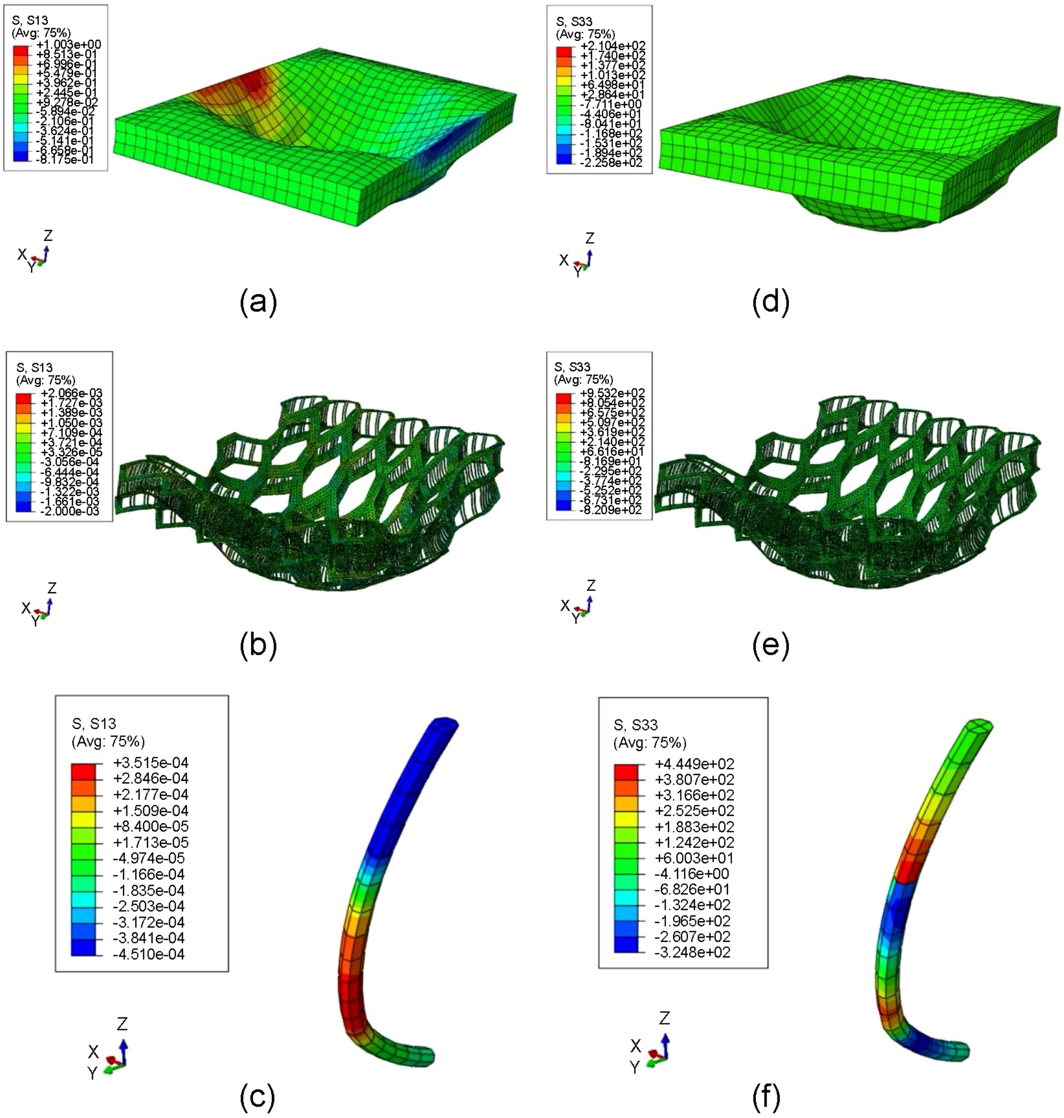

Fig. 14. Stresses in BLF sample: (a) shear stress in composite, (b) shear stress in reinforcement, (c) shear stress on central pile yarn, (d) normal stress in matrix, (e) normal stress in reinforcement, and (f) normal stress on central pile yarn.

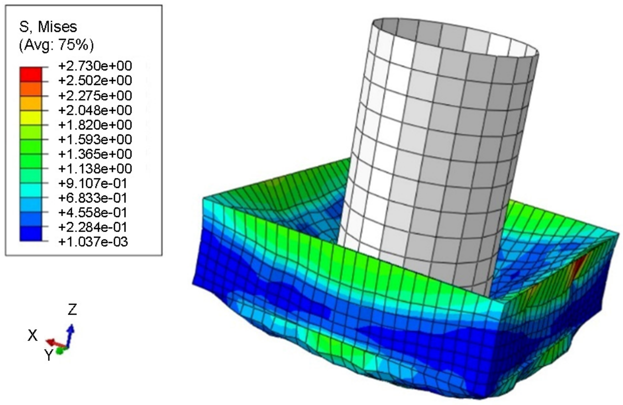

Fig. 15. Von Mises stress in BHF sample.

ABAQUS CAE/2022 commercial package. Mesh type of C3D8R was applied for both the WKSF and foam. Different mesh size for pile yarns and layers was used. Elastic properties of polyester were given to the reinforcement and the properties of low-density foam was given to the matrix. Five types of foam-based sandwich composites were modeled as presented in Table II.

The results of low-velocity impact simulations for different samples are shown in Figs. 13 to 21. The values of Mises stress, value and positions of maximum normal and shear stress in the composite samples also normal and shear stress in pile-yarns at center of impact area are discussed in the following. Fig. 12 shows the magnitude

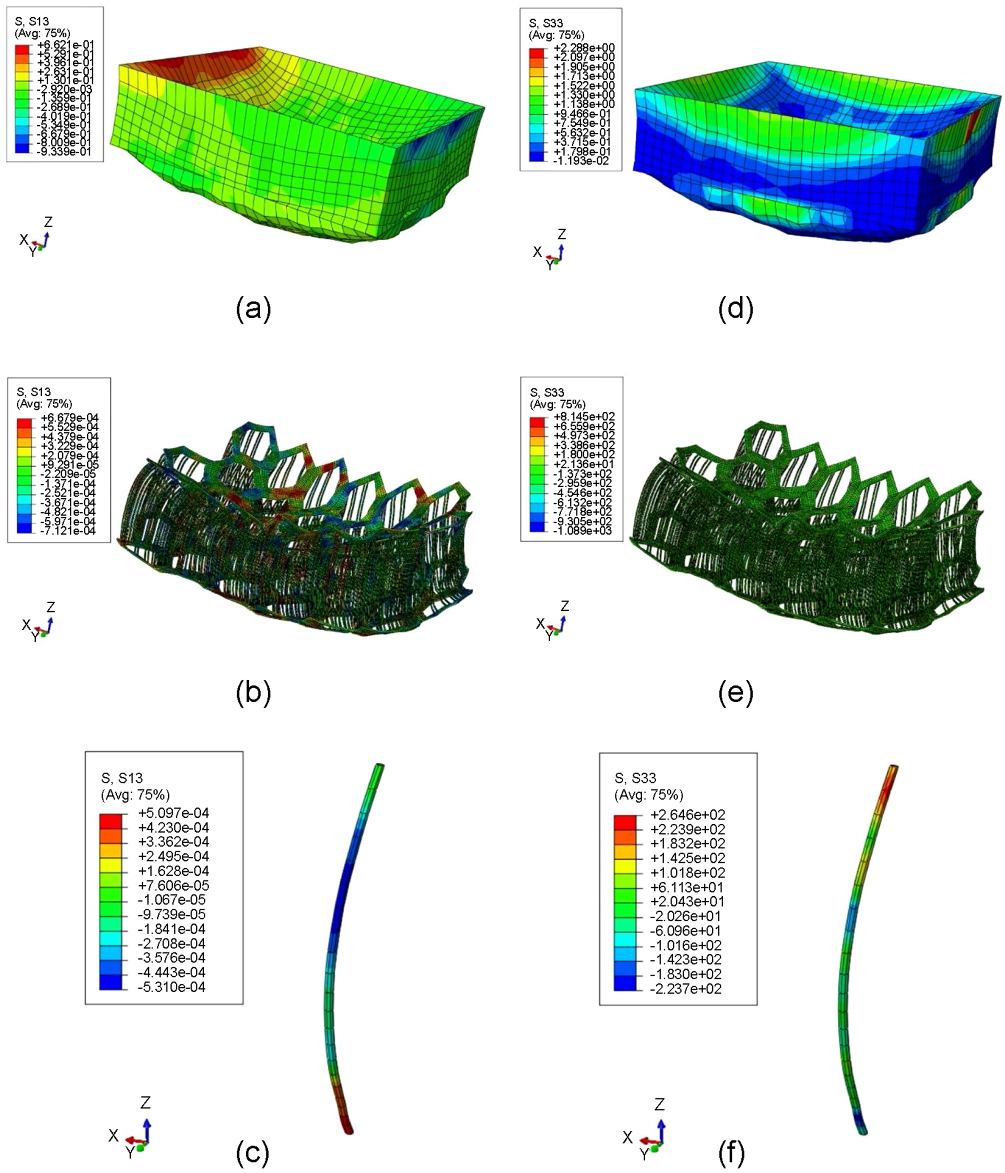

Fig. 16. Stresses in BHF sample: (a) shear stress in composite, (b) shear stress in reinforcement, (c) shear stress on central pile yarn, (d) normal stress in matrix, (e) normal stress in reinforcement, and (f) normal stress on central pile yarn.

and distribution of von Mises stress created on the BLF sample. As indicated, the maximum stress value occurs continuously at the outer edges of the foam.

As can be seen from Fig. 13a, the maximum shear stress occurs in outer edge of composite box. Also, the lateral movement of the reinforcing fabric and the membrane deformation of the foam can be observed in this Figs. 14a and 14b. As shown in Fig. 14b, the maximum of normal stresses occurs after low-velocity impact in BLF composite. Figs. 14c and 14f demonstrate the distribution of shear and normal stress in the pile yarn at the central of contact area, along with the stress distribution and deformation changes due to the impact load. The maximum occurs at the center of the pile yarn. Additionally, the joint area of the pile yarn with the bottom layer withstands high shear stress. Exactly contrary to the location of the maximum shear stress, the highest normal stress value occurs at the joint areas between the pile thread and the layers.

Fig. 15 depicts the values of von Mises stress created on the BHF samples after the impact of the impactor. The maximum value of von Mises stress is equal to 2.73 Mpa. Given that the hexagonal cell positions of the reinforcement are face to face, the stress distribution is approximately uniform throughout all parts of the composite.

Fig. 16 represents the magnitude and distribution of stresses in the BHF composite and central pile yarn. This maximum shear stress according to Fig. 16a occurred in the border strip of the foam box, as expected. Also, Fig. 16b shows the magnitude and distribution of shear stress in the BHF fabric outside of the foam. The maximum value of this stress occurred at the pile yarn or the location where the base meshes are connected to each other. The shear stress in the composite specimen reinforced with BHF is lower than that of the BLF specimen. Undoubtedly, the most important factor in this issue is the greater thickness and higher impact resistance of the BHF sample. According to Fig. 16d, the maximum normal stress value in the matrix of BHF sample has occurred in the edge of matrix. Also, based on Fig 16e, the distribution of normal stress in the reinforcement shows that the normal stress is distributed uniformly. The value and distribution of shear and normal stresses on the pile yarns of BHF sample is shown in Figs. 16c and 16f. Considering the contour of shear stress in Fig. 16c, the stress distribution is higher in the upper and lower parts of the piles, contrary to the pile yarns in the BLF sample. This difference in stress location can be attributed to the structure of the BHF reinforcing fabric sample. The maximum shear stress value in the BHF pile yarn is slightly lower than the shear stress in the pile yarn of BLF according to Fig. 14c. According to Fig. 16f, the maximum normal stress occurred at the connection point

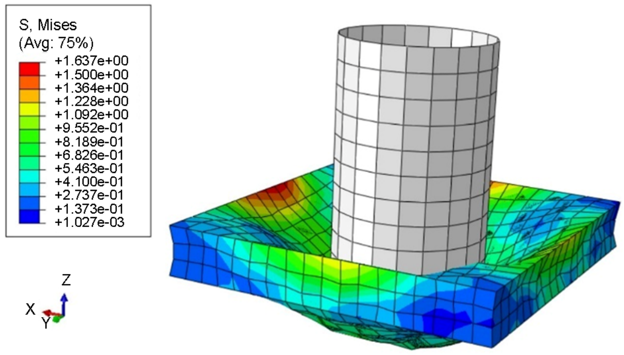

Fig. 17. Von Mises stress in BLN sample.

of the pile yarn with higher wall.

Fig. 17 shows the von Mises stress distribution in a BLN sample. The maximum stress value is equal to 1.63 MPa, which occurs in the vicinity of the impact area, unlike the BLF and BHF samples that were examined.

In non-facing position, a lateral movement happens when they are subjected to the normal load like impact force as shown in Fig. 18.

Fig. 19a shows the magnitude and distribution of shear stress in the BLN sample. It appears that the maximum shear stress in BLN sample is less than that of BLF sample which is attributed to the non-facing position of the cell in WKSF structures. Furthermore, according to Fig. 19b, the maximum shear stress value in the reinforcement mainly occurs at the pile yarns. According to Fig. 19d. The distribution of normal stress in this specimen is almost uniform as shown in this Figure. As illustrated in Fig. 19e, the maximum normal stress occurs at the junction of the wall meshes and is somewhat equal to the normal stress throughout the composite. The shear and normal stress created on pile yarns of BLN sample is shown in Figs. 19c and 19f. Referring to Fig. 19c, the highest shear stress in the pile yarn occurred at the middle of them. Additionally, Fig. 19f shows the highest amount of normal stress in the pile yarn.

The magnitude and distribution of von Mises stress in BHN sample are shown in Fig. 20. According to this figure,

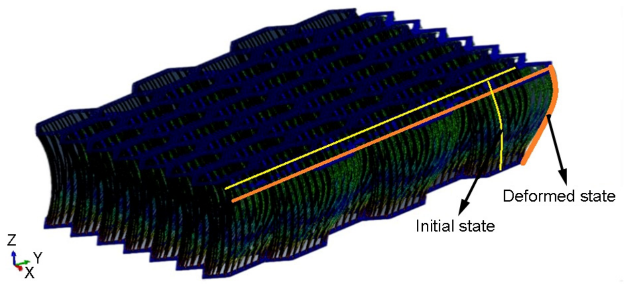

Fig. 18. Lateral movement of top layer in non-facing cells subjected to normal load.

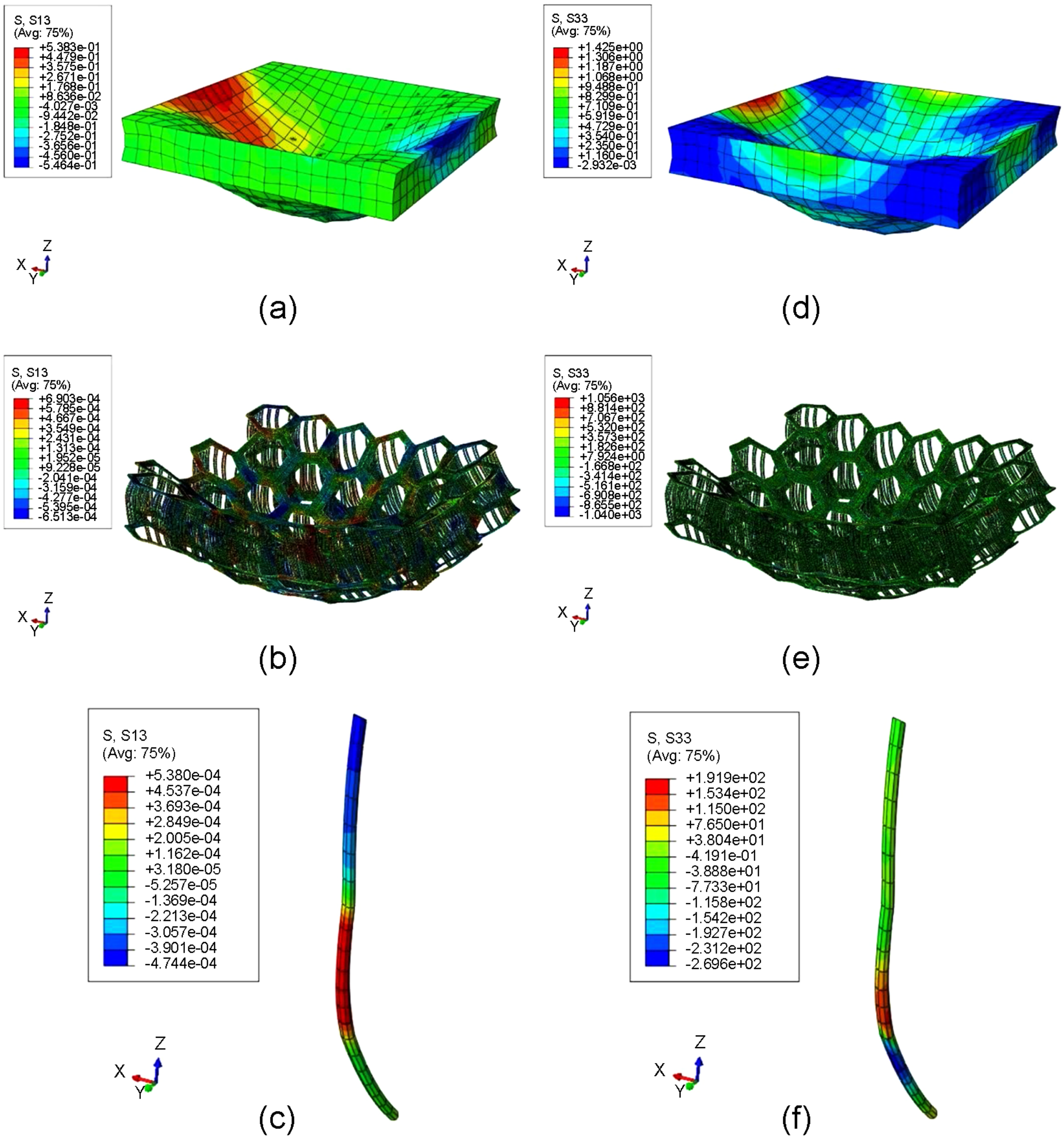

Fig. 19. Stresses in BLN sample: (a) shear stress in composite, (b) shear stress in reinforcement, (c) shear stress on central pile yarn, (d) normal stress in matrix, (e) normal stress in reinforcement, and (f) normal stress on central pile yarn.

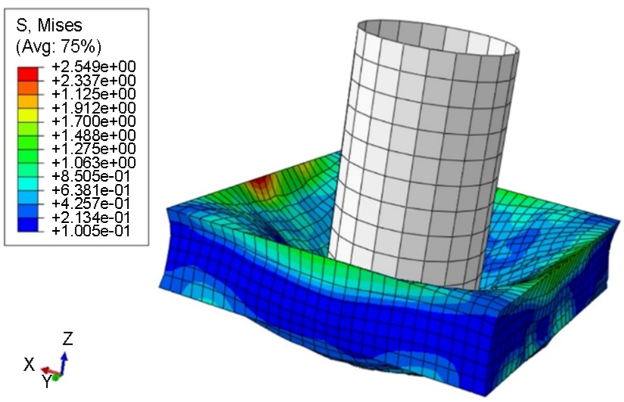

Fig. 20. Von Mises stress in BHN sample.

the maximum value of von Mises stress is 2.49 MPa and occurred at the edge of the composite.

Fig. 21a shows the maximum shear stress value BHN composite and its location is at the outer edge of the foam box. Also, the minimum shear stress value occurs in the opposite side that is due to the lateral movement of non-facing structures. Fig. 21b shows that the matrix has main role in bearing shear stress. According to Figs. 21d and 21e, the maximum normal stress has occurred in the matrix and reinforcement of BHN sample. It seems that the distribution of normal stress in this specimen is uniform in most parts of the composite and reinforcing fabric, and no specific critical point is observed. Figs. 21c and 21f show

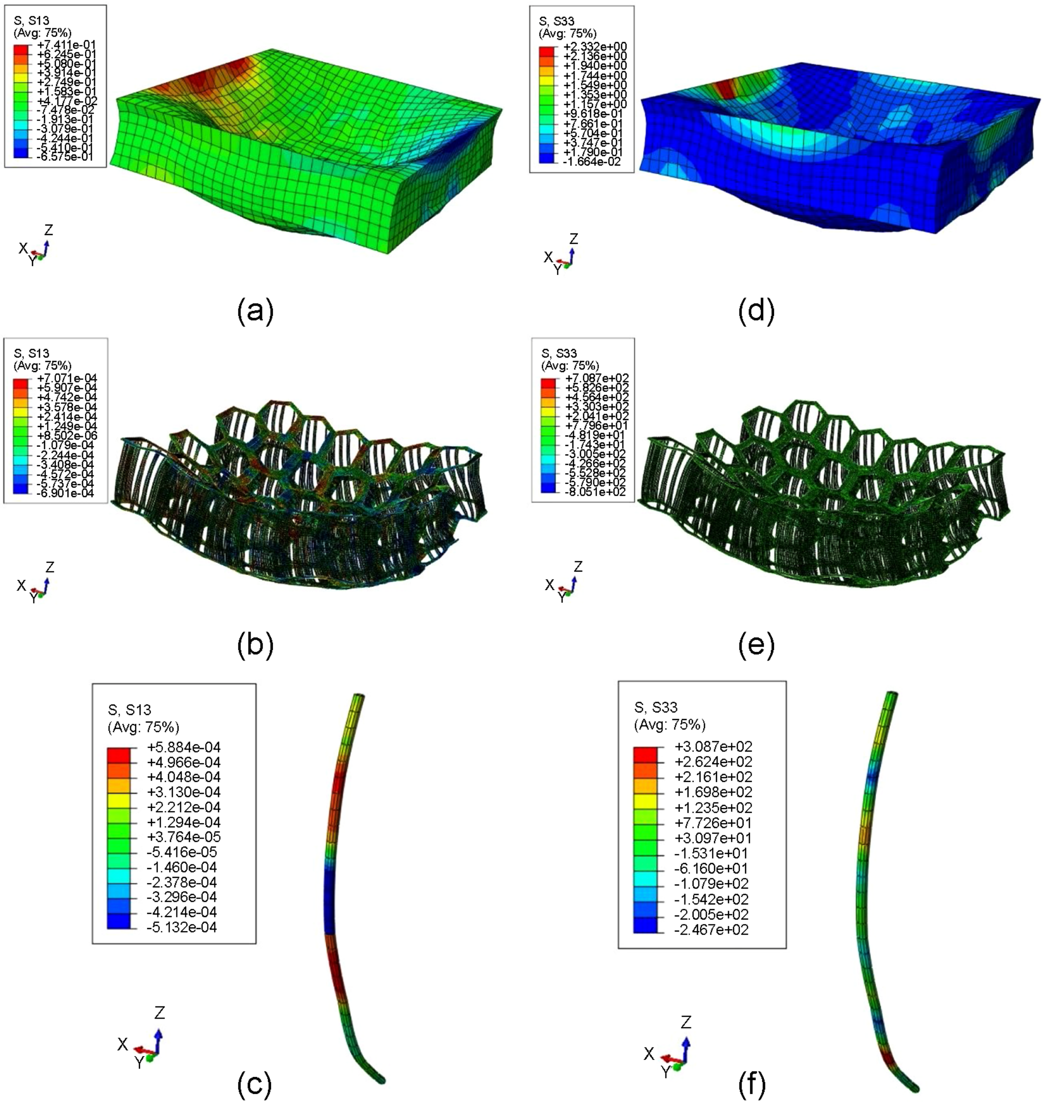

Fig. 21. Stresses in BHN sample: (a) shear stress in composite, (b) shear stress in reinforcement, (c) shear stress on central pile yarn, (d) normal stress in matrix, (e) normal stress in reinforcement, and (f) normal stress on central pile yarn.

the maximum shear and normal stresses created on the pile yarn. Based on Fig. 21c, the shear stress has occurred in

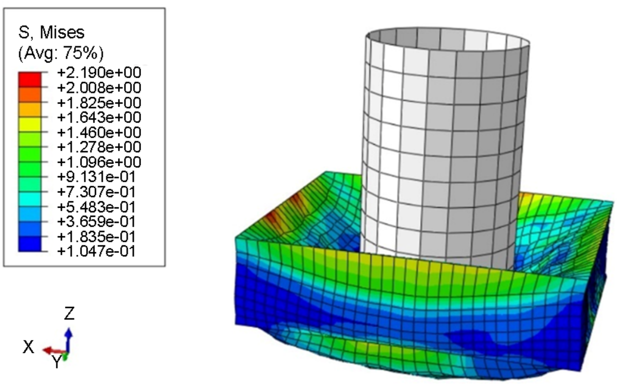

Fig. 22. Von Mises stress in SHN sample.

the lower half of this pile yarn. Also, the maximum normal stress value is slightly higher than the maximum normal stress in the pile yarn of the BLN sample. It seems that doubling the thickness in the BHN specimen has resulted in a higher maximum normal stress than the BLN sample.

The value and distribution of von Mises stress in the SHN foam-based composite is shown in Fig. 22. As indicated, the maximum value of Mises stress is equal to 2.19 MPa and has occurred at the edges of the composite.

Fig. 23a shows that the maximum shear stress in SHN sample has occurred at the outer edge of the foam box. In addition, the minimum shear stress has been observed opposite to the maximum value, which can be attributed to the lateral movement of the reinforcement as shown in Fig. 23a. Fig. 23b shows the maximum shear stress on the

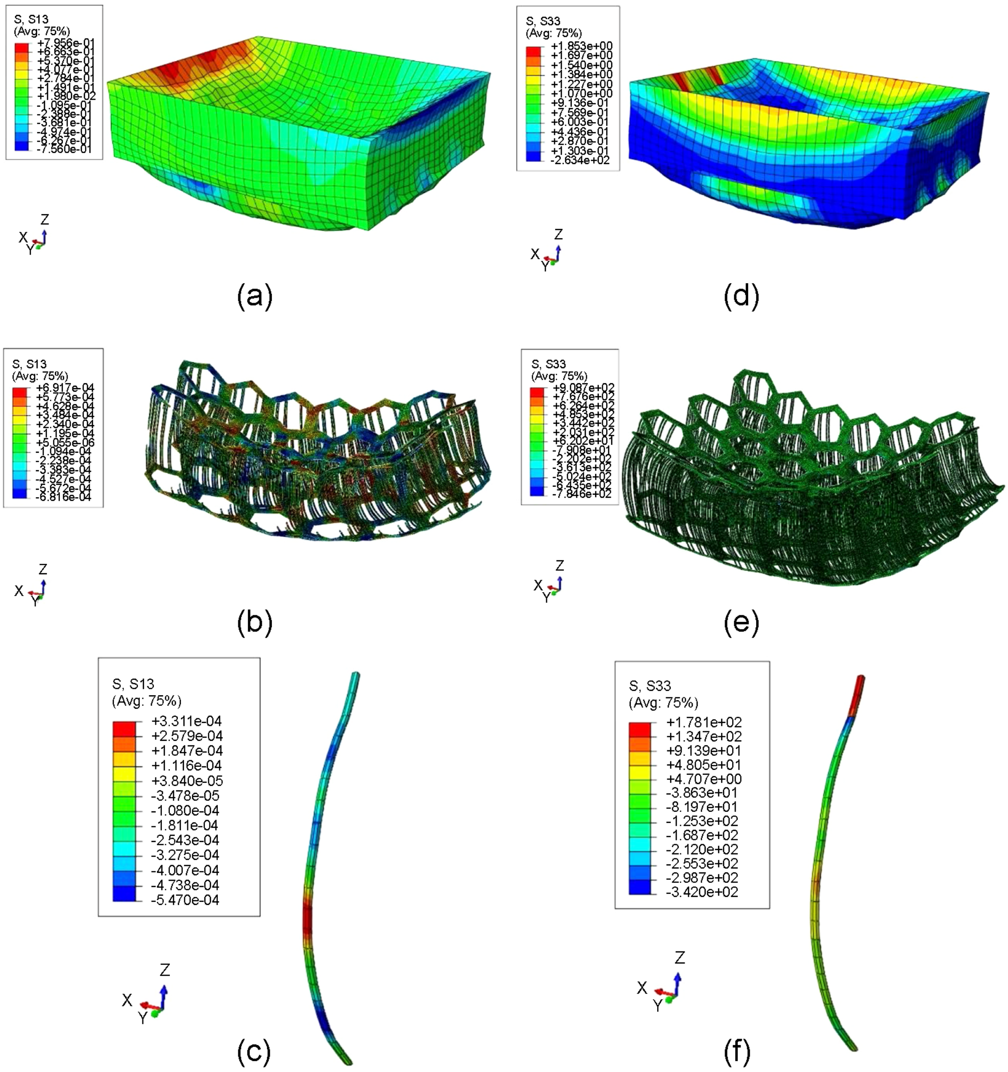

Fig. 23. Stresses in SHN sample: (a) shear stress in matrix, (b) shear stress in reinforcement, (c) shear stress on central pile yarn, (d) normal stress in composite, (e) normal stress in reinforcement, and (f) normal stress on central pile yarn.

reinforcement of the SHN. The location of this maximum shear stress occurs at the connection point of the layer and the pile yarns. The maximum value of normal stress in the matrix and reinforcement are shown in Figs. 23d and 23e. Also Figs. 23c and 23f show the shear and normal stresses created on the pile yarns of the SHN sample. As can be seen in Fig. 23c, the value of this maximum shear stress is slightly less than that of the BHN sample. It appears that by decreasing the cell-size in the SHN sample and consequently the increase in the density of the cells, more elements absorb the impact energy. Also, according to Fig. 23f, the maximum normal stress occurred on the central pile yarn of the SHN

TABLE III
THE RESULTS OF NUMERICAL SIMULATION OF LOW-VELOCITY IMPACT

	Shear stress (kPa)			Normal stress (MPa)			Von Mises (MPa)
	Composite	Fabric	Pile yarn	Matrix	Fabric	Pile yarn	Composite
BLF	1003	0.206	0.35	210.4	953.1	444.9	2.24
BHF	662.1	0.667	0.51	228.8	841.5	264.7	2.73
BLN	538.9	0.69	0.53	142.5	1056.3	191.9	1.63
BHN	254.9	0.741	0.71	233.2	708.7	387.5	2.54
SHN	795.6	0.691	0.34	185.3	908.7	178.1	2.19

TABLE IV
COMPARISON OF NUMERICAL AND EXPERIMENTAL MAXIMUM ACCELERATION OF IMPACTOR

Sample's code	Maximum acceleration of impactor ($m.s^{-2}$)		Error (%)
	Experimental	Numerical	
SHN	136.2	122.8	9.8
BLN	49.9	51.3	2.8
BLF	46.9	50.6	7.1
BHF	61.9	58.2	6.0
BHN	91.3	99.4	8.8

sample at the connecting point to the top layer.

Table III shows the results of numerical simulation as shear and normal stresses in different parts of samples.

In addition, Table IV shows the comparison between numerical and experimental maximum acceleration of impactor for different samples. As presented, there is a reasonable agreement between numerical and experimental results.

IV. CONCLUSION

A numerical study was performed to simulate the low-velocity impact behavior of polyurethane foam-based composites reinforced with warp-knitted spacer fabrics (WKSFs). For this purpose, easy-to-use mathematical equations were developed to define the geometry of WKSFs. The structure of reinforcements was modeled using Python programming language in ABAQUS software. The low-velocity impact behavior of modeled composites was numerically simulated. Finally, the actual experimental resulted from the drop hammer test. The results have shown that:

- On average, by increasing the thickness of reinforcements (WKSF) from 7 mm to 14 mm, the maximum impact acceleration increased by 76.3%.
-The average maximum impact acceleration in composite samples with non-facing position of hexagonal cells is 58.2% higher than the facing position.
- The average maximum impact acceleration in samples with small cell-sized is 62.2% higher than samples with big cell-sized.
- Comparison between the numerical and experimental results confirmed that the generated model and numerical simulation could reasonably predict the low-velocity impact behavior of foam-based composites reinforced with WKSF.

REFERENCES

[1] F.T. Peirce, "The geometry of cloth structure", *J. Text. Inst. Trans.*, vol. 12, no. 3, pp. T45-T96, 1937.

[2] G. Leaf and A. Glaskin, "The geometry of a plain knitted loop", *J. Text. Inst. Transactions*, vol. 46, no. 9, pp. T587-T605, 1955.

[3] A. Kemp, "An extension of Peirce's cloth geometry to the treatment of non-circular threads", *J. Text. Inst. Trans.*, vol. 49, no. 1, pp. T44-T48, 1958.

[4] D. Munden, "The geometry and dimensional properties of plain-knit fabrics", *J. Text. Inst. Trans.*, vol. 50, no. 7, pp. T448-T71, 1959.

[5] J. Hearle and W. Shanahan, "An energy method for calculations in fabric mechanics. Part I: principles of the method", *J. Text. Inst.*, vol. 69, no. 4, pp. 81-91, 1978.

[6] S.G. Vassiliadis, A.E. Kallivretaki, and C.G. Provatidis, "Geometrical modelling of plain weft knitted fabrics", *Indian J. Fibre Text. Res.*, vol. 32, pp. 62-71, 2007.

[7] M.K. Dolatabadi and R. Kovař, "Geometry of plain weave fabric under shear deformation. Part II: 3D model of plain weave fabric before deformation", *J. Text. Inst.*, vol. 100, no. 5, pp. 381-386, 2009.

[8] A.A.A. Jeddi, H.R. Karimi, and A. Rastgoo, "Theoretical analysis of load-extension behaviour of plain-weft-knitted fabric", *J. Text. Inst.*, vol. 100, no. 1, pp. 18-27, 2009.

[9] H. Dabiryan and A.A.A. Jeddi, "Analysis of warp knitted fabric structure. Part I: a 3D straight line model for warp knitted fabrics", *J. Text. Inst.*, vol. 102, no. 12, pp. 1065-74, 2011.

[10] Y. Kyosev, "Generalized geometric modeling of tubular and flat braided structures with arbitrary floating length and multiple filaments", *Text. Res. J.*, vol. 86, no. 12, pp. 1270, 2015.

[11] A. Kurbak, "Geometrical models for weft-knitted spacer fabrics", *Text. Res. J.*, vol. 87, no. 4, pp. 409-423, 2017.

[12] K. Delavari and H. Dabiryan, "Mathematical and numerical simulation of geometry and mechanical behavior of sandwich composites reinforced with 1×1-rib-gaiting weft-knitted spacer fabric; compressional behavior", *Compos. Struct.*, vol. 268, pp. 113952, 2021.

[13] D.M. Schwaber, "Impact behavior of polymeric foams: a review", *Polym. Plast. Technol. Eng.*, vol. 2, no. 2, pp. 231-249, 1973.

[14] L.J. Gibson, M.F. Ashby, G.S. Schajer, and C.I. Robertson, "The mechanics of two-dimensional cellular materials", *Proc. R. Soc. Loud. A*, vol. 382, pp. 25-42, 1982.

[15] T. Allen, J. Shepherd, T.A.M. Hewage, T. Senior, L. Foster, and A. Alderson, "Low-kinetic energy impact response of auxetic and conventional open-cell

polyurethane foams", *Phys. Status Solidi Basic Res.*, vol. 252, no. 7, pp. 1631-1639, 2015.

[16] H. Dabiryan, F. Hasanalizade, and M. Sadighi, "Low-velocity impact behavior of composites reinforced with weft-knitted spacer glass fabrics", *J. Ind. Text.*, vol. 49, no. 4, pp. 465-483, 2019.

[17] N.W. Li, K.L. Yick, and A. Yu, "Novel weft-knitted spacer structure with silicone tube and foam inlays for cushioning insoles", *J. Ind. Text.*, vol. 51, no. 4, pp. 6463S-6483S, 2022.

[18] F. Hasanalizade and H. Dabiryan, "Theoretical modeling of low-velocity impact behavior of sandwich-structured composites reinforced with weft-knitted spacer fabric", *J. Ind. Text.*, vol. 52, pp. 1-21, 2022.

[19] C. Zhi, M. Du, Z. Sun, M. Wu, X. He, J. Meng, and L. Yu, "Warp-knitted spacer fabric reinforced syntactic foam: a compression modulus meso-mechanics theoretical model and experimental verification", *Polymers (Basel)*, vol. 12, no. 2, 2020.

[20] K. Delavari and H. Dabiryan, "Effect of Z-fiber orientation on the bending behavior of sandwich-structured composite: Numerical and experimental study", *Compos. Struct.*, vol. 256, pp. 113140, 2021.

[21] V. Ghorbani, A.A.A. Jeddi, and H. Dabiryan, "Theoretical and experimental investigation of tensile properties of net warp-knitted spacer fabrics", *J. Text. Inst.*, vol. 111, no. 4, pp. 518-528, 2020.